# Low-signal electrical circuit of a Schottky diode according to microwave spectrometry

© A.N. Reznik, N.V. Vostokov

Institute for Physics of Microstructures, Russian Academy of Sciences, 603950 Nizhny Novgorod, Russia

E-mail: reznik@ipm.sci-nnov.ru

Received March 26, 2025 Revised June 23, 2025 Accepted June 23, 2025

Homogeneous n-Si and structured n-GaAs samples with a system of concentric barrier contacts on the surface were studied by microwave volt-impedance spectroscopy. Based on measurements in the frequency range of  $f=0.01-67\,\mathrm{GHz}$  with a lateral resolution of  $20-50\,\mathrm{microns}$ , the spectra of the complex impedance Z(f,U) were reconstructed for the Si sample (U) is the bias voltage at the contact). The electrophysical characteristics of the semiconductor such as the type, concentration and mobility of free charge carriers, specific electrical conductivity, and barrier potential difference are determined from the spectra. Excessive resistance and a capacity drop  $C(f\to 0)>C(f\to \infty)$  of the Schottky contact were detected in the frequency range of  $0.1-20\,\mathrm{GHz}$ . A low-signal electrical Schottky diode circuit is proposed, characterized by two time scales — low-frequency  $\tau_l=(0.5-1)\cdot 10^{-9}\,\mathrm{s}$  and high-frequency  $\tau_h=(3-4)\cdot 10^{-11}\,\mathrm{s}$ . In addition to the previous studies, the microwave spectrum Z(f,U=0) was measured after heating GaAs sample to a temperature of up to  $T=100\,^{\circ}\mathrm{C}$  and at low frequencies of  $10^2-10^6\,\mathrm{Hz}$  with a temperature sweep across  $T=77-345\,\mathrm{K}$ . According to the totality of all studies, the hypothesis put forward earlier is that the observed microwave effects are related to the recharge of deep states (traps) did not find any confirmation. Another interpretation is proposed, linking the effects with the peculiarities of charge carrier transport in the depleted layer of the Schottky contact. The possibilities of physical substantiation of this mechanism are discussed.

**Keywords:** microwave range, probe station, impedance, semiconductor, barrier contact, electrophysical characteristics, carrier transport, excess resistance.

DOI: 10.61011/SC.2025.02.61361.7727

#### 1. Introduction

Metal-semiconductor contact with a Schottky barrier is widely used in microwave (MW) detectors, mixers, transistors, etc. [1]. The Schottky contact (SC) is also formed to measure the concentration of free charge carriers in semiconductors. In the latter case, a constant bias voltage is applied to the contact U and the SC capacitance  $C_d(U)$  is measured (C-V-method) [2]. An MW diagnostic method (a partial equivalent of C-V), called volt-impedance (Z-V)spectroscopy, was proposed and tested in Refs. [3-6] It was demonstrated that is possible to determine the main electrophysical characteristics of a semiconductor such as the type of free carriers, their concentration n and mobility  $\mu$ , and specific electrical conductivity  $\sigma$ . The desired parameters are retrieved from measurements of the frequency f spectrum of the complex impedance Z(f, U)of the studied sample. The main advantage of Z-Vdiagnostics is the locality of measurements. The lateral resolution was 10-60 microns in Refs. [4-6]. The key element of the spectrometer used is the probe station (PS). Since the mid 1980s, the PS has become one of the main commercially available devices designed for MW testing of integrated circuit elements of micron sizes directly on a plate [7,8]. The main task of the PS measurements is to construct an equivalent circuit of the studied device. The

same problem is solved in this paper with respect to the Schottky diode. We also confirm the potential of the Z-V-method using a new silicon-based sample.

An alternative technique for local diagnosis is scanning microwave microscopy (SMM). Currently, testing of semiconductor materials and solid-state microelectronics devices is considered as the most promising field of application of the relevant technology. Review publications [9–12] contain links to original studies of SMM. The authors of a number of papers make an optimistic conclusion about the possibility of determining the concentration of charge carriers in a semiconductor with a nanometer (30–50 nm) resolution. The issue of semiconductor diagnostics using micro- and nanoresolution SMM is discussed in the conclusion, which also provides a comparison with the local MW spectroscopy based on PS.

Along with solving the main problem, excessive resistance was found in Refs. [5,6] for GaAs samples in the range of  $0.1-20\,\mathrm{GHz}$ , which is not described by the classical equivalent SC circuit shown in Figure 1, a, where  $R_c$  is the DC resistance, r is the spreading resistance in the quasi-neutral region of a semiconductor under a depleted SC layer  $(r \ll R_c)$ . We have  $R(f) = Re\left(Z(f,U)\right) \approx r$  in the MW range, according to the scheme in Figure 1, a, whereas the observed exceedance of R(f) relative to r reached 1-2 orders of magnitude. Excess resistance is

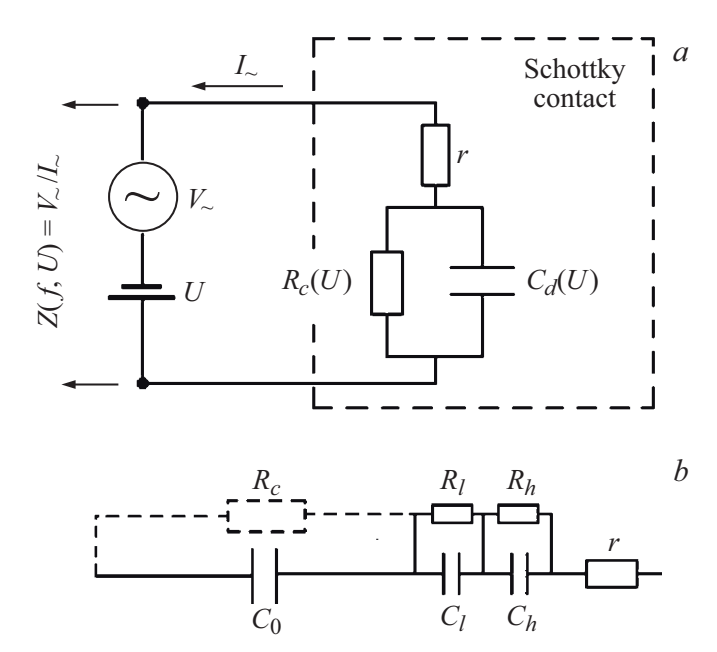


**Figure 1.** a — equivalent 1s SC circuit. b — 2s scheme for microwave and low-frequency bands.

important for many devices using SC. For instance, this resistance can determine the Joule loss at the difference frequency in millimeter and submillimeter range mixers. A hypothesis was put forward in the Refs. [5,6] according to which the detected effect could be associated with the recharge of deep states (traps), leading to additional MW losses, which is why the circuit in Figure 1, a is transformed by introducing an impedance  $Z_t = R_t - i/\omega C_t$  parallel to the capacitance  $C_d$ . Traps in semiconductors have been actively studied since the 1960s at low frequencies for SC of sufficiently large-diameter a > 300 microns [7,13–19]. In our case, the effect was observed at room temperature with an extremely short characteristic time  $\tau \sim 4 \cdot 10^{-11} \, \text{s}$ . In this work, a number of additional studies were performed on the GaAs sample studied in Ref. [6], as well as a new sample made from a single crystal plate of n-Si (a standard substrate). The data obtained here casts doubt on the trap hypothesis regarding the effects we observed. this regard, another interpretation has been put forward, linking the excess resistance with the transport of residual charge carriers in the depleted SC layer. The corresponding transformation of the SC scheme in Figure 1, a will allow taking into account the effects observed by us.

## 2. Measurement methods and examined samples

The GaAs sample (see also Ref. [6]) is a sulfur-doped film grown on a conductive substrate of  $n^+$ -GaAs with a buffer sublayer. According to the data of Z-V-diagnostic the concentration and mobility of carriers in the film were  $n_f = 4.1 \cdot 10^{16} \, \mathrm{cm}^{-3}$ ,  $\mu_f = 1.2 \cdot 10^3 \, \mathrm{cm}^2/(\mathrm{V} \cdot \mathrm{s})$ ,

barrier potential difference  $U_c=0.88\,\mathrm{V}$ . It should be noted that standard Hall measurements of the electrophysical parameters of the film were not possible due to the shunting action of the substrate.

A new sample phosphorus-doped substrate n-Si, on the surface of which a system of concentric metal contacts (antenna system) is formed. Measurements of the impedance spectrum Z(f, U) were performed on A1, A2 antennas with an inner and outer diameter of a metallization-free ring separating the contacts a = 20, 50 microns and b = 40, 70 microns, respectively. MW measurements were performed using Cascade Microtech PS and the Agilent E8361 A vector network analyzer in the range of 0.01-67 GHz (1600 points with a logarithmic Voltage of U = 0, 0.5, 1...4.5 V was applied between the external and internal contact pads of the antenna with a negative bias on the internal contact (metal disk). A depleted layer with a thickness of d(U) ( $d \ll a$ ) is formed inside a semiconductor in the area of contact with a metal antenna. Measuring the imaginary part of the impedance  $Im(Z(f, U)) = -X(f, U) = -1/(2\pi f C_d(U))$ allows restoring the function d(U), which is conventionally related to the concentration n in the quasi-neutral region. The resistance spectrum of R(f, U) = Re(Z(f, U)) provides information about the conductivity  $\sigma$ , which determines the mobility  $\mu$ . The corresponding results and the necessary ratios will be given below. A detailed description of the measurement procedure is given in Ref. [6], photos of the PS, MW probe and antenna system are given in the article [5]. The following values of the electrophysical parameters of the Si sample were obtained via Hall measurements in Van der Pauw geometry:  $n = 9.75 \cdot 10^{16} \,\mathrm{cm}^{-3}$ ,  $\mu = 783 \,\mathrm{cm}^2/(\mathrm{V} \cdot \mathrm{s}), \, \sigma = 12.2 \,(\mathrm{Ohm} \cdot \mathrm{cm})^{-1}$ . Additionally, MW measurements were performed when the GaAs sample was heated using the A200H+25 thermostat from the Apart from room temperature  $T = 24 \,^{\circ}\text{C}$  the spectrum Z(f, U = 0) was obtained at T = 100 °C. The lateral resolution of Z-V method is determined by the diameter a of the antenna's inner contact. The external AC contact of the antenna is short-circuited with the quasineutral region of the semiconductor under the depleted layer, since its area is  $S_b \gg S_a = \pi a^2/4$ . A more detailed resolution analysis is given in Ref. [6].

Let's pay attention to an important circumstance that accompanies MW measurements with the help of the PS. To restore the impedance spectrum Z(f), it is necessary to perform a single-port calibration of the probe, for which the manufacturer includes a set of standard planar loads with impedances  $Z = -i\infty$  (O — open), 0 (S — short), 50 Ohm (M — matched) in the entire operating range of the PS. The corresponding probe calibration method [8], often referred to as OSM, is also widely used in the vector network analysis technique [20]. Having applied the OSM method to the GaAs sample according to the protocol, we encountered an unexpected problem. There were significant errors in the measured resistance spectrum R(f) in the most informative part of the operating range f > 5 GHz. An

alternative AK measurement method has been developed in Ref. [6] for eliminating errors that does not use impedance standards. AK spectrometry models a probe by a segment of a matched two-wire line. The electrodynamic parameters of the line are determined by measuring the MW spectrum of the reflection coefficient of the probe in the absence of its contact with the test sample (Air mode). The cause of OSM errors was established in Ref. [21] (as it turned out, caused by imperfect parameters of standard loads), and a more detailed study of the AK method was performed. In this work, we also applied the AK method in the study of the Si sample. The corresponding description is given in the Appendix, which draws attention to the expediency of specific correction of experimental data in AK measurements.

In low-frequency (LF) measurements, the admittance  $Y = Z^{-1}$  of the GaAs sample was recorded using a Quad Tech 7600 precision LCR meter at 9 frequencies  $10^2$ ,  $3 \cdot 10^2 \dots 3 \cdot 10^5$ ,  $10^6$  Hz at U = 0 with a temperature sweeping. The electrical contacts were located on opposite sides of the semiconductor wafer. We used a contact with a diameter a = 400 microns in the antenna block. Low-temperature measurements were carried out in a Dewar nitrogen vessel. Two measurement cycles were performed in the temperature range of 77-298, 132-347 K in increments of 0.5-1.5, 1.5-3 K, respectively. The sample holder was heated in the latter case. At room temperature, the dependence  $C(U) = \text{Im}(Y)/\omega$  was measured at the negative bias voltages U specified above to determine the concentration of free carriers  $n_f$  using the C-V method.

#### 3. Research results

#### 3.1. MW measurements

In the process of AK diagnostics of the Si sample, measurements of the complex reflection coefficient at the probe input  $\Gamma(f)$  (S11 from the system of S-parameters) in the Air mode and in contact with the A1 and A2 antennas of the sample were performed in a single cycle. The electrodynamic characteristics of the probe modeling line — electrical length  $l_e(f)$  and attenuation parameter  $\delta(f)$  are determined (see Appendix). The impedance spectrum is calculated using the formulas:

$$Z(f) = Z_{CM} \frac{1 + \Psi(f)}{1 - \Psi(f)},$$
 (1)

$$\Psi(f) = \exp\left\{i\,\frac{2\omega l_e(f)(1-i\delta(f))}{c}\,\Gamma(f)\right\}, \qquad (2)$$

where  $\omega = 2\pi f$ , c is the speed of light,  $Z_{CM} = 50$  Ohms is the wave impedance of the line. When processing the experimental data, the modified spectra  $\Gamma(f)$  given in the Appendix were used. A detailed description of the measurement methodology is given in Ref. [21].

Figure 2 shows the resistance spectra of R(f,U) for each antenna, reconstructed from experimental data at U=0, 4.5 V. The given spectra for the Si sample are quite similar to the spectra for the GaAs structure studied in Ref. [6]. In the high frequency range of  $f>20\,\mathrm{GHz}$ , we can see the spectrum R(f) transition to the spreading resistance r(f) that is independent on U and describes the MW current dissipation in the quasi-neutral region of a semiconductor with a conductivity  $\sigma$ . We calculated it according to the formula [22]

$$r(f) = \frac{1}{2\pi} \left[ \sqrt{\frac{\omega\mu_0}{2\sigma}} \ln\left(\frac{b}{a}\right) + \frac{2}{\sigma a} \arctan\left(\frac{b}{a}\right) \right], \quad (3)$$

where  $\mu_0$  is the magnetic constant of the vacuum. The curves r(f) in Figure 2 are plotted at  $\sigma = 9.5$  (A1), 8.5 (Ohm·cm)<sup>-1</sup> (A2), in satisfactory agreement with the Hall measurements. The obtained spectra R(f, U) in the range of 0.1-10 GHz demonstrate excessive resistance, and just as in Ref. [6], we see two time scales —  $\tau_h$ ,  $\tau_l$  ( $\tau_h \ll \tau_l$ ).

The impedance spectrum Z(f, U) will be approximated by a two-scale (2s) model, discussed in Sec. 4:

$$Z(f,U) = -\frac{i}{\omega C_0(U)} + \frac{R_l(U)}{1 + i\omega\tau_l} + \frac{R_h(U)}{1 + i\omega\tau_h} + r(f).$$
(4)

The results of the calculation of the spectra R(f) using the formula (4) are shown in Figure 2. The values of the function (4) parameters for U = 0, 4.5 V are given in the table. Once again, we emphasize that the spectrum described by the expression (4) does not correspond to the equivalent scheme in Figure 1, a. In this circuit, the DC resistance measured is  $r_c = R_c \cdot S_a \approx 3 \cdot 10^3 - 10^5 \, \text{Ohm} \cdot \text{cm}^2$ It is possible to assume  $R_c \to \infty$  in the at U < 0. considered frequency range,  $f > 0.01 \,\text{GHz}$ , i.e., we would have  $Z(f) = -i/(\omega C_d) + r(f)$  according to the scheme in Figure 1, a. The difference between the scheme (4)from Figure 1, a — serial connection to the capacitance  $C_0$  of two parallel connected resistances  $R_{l,h}$  with capacitances  $C_{l,h} = \tau_{l,h}/R_{l,h}$  (see Figure 1, b). The summands  $R_{l,h}/(1+i\omega\tau_{l,h})$  describe the excess resistance in the model (4), and also determine the correction  $\Delta C(f)$  to the capacitance  $C_0$ . The experimental capacitance spectra of both contacts  $C(f, U) = 1/[\omega X(f, U)]$  are shown in Figure 3, which also shows the calculation results using the formula (4) with the parameters from the table. As can be seen from Figures 2 and 3, the model (4) describes the obtained spectra well. The transition  $C_0 \to C_\infty = C_0 - \Delta C(f) < C_0$ , which was not observed for the GaAs sample in Ref. [6], is clearly recorded in the spectra C(f) in Figure 3. It should be noted that the capacity  $C_{\infty}$  is not a parameter of the model (4), i.e., the experimentally observed transition  $C_0 \to C_\infty$  is automatically obtained in this model after determining the parameters  $R_{l,h}$ ,  $\tau_{l,h}$ ,  $C_0$ .

In the region of low  $(f < 0.5\,\mathrm{GHz})$  and high  $(f > 50\,\mathrm{GHz})$  frequencies, the spread of the restored values of R and C is quite large, which is especially typical for the

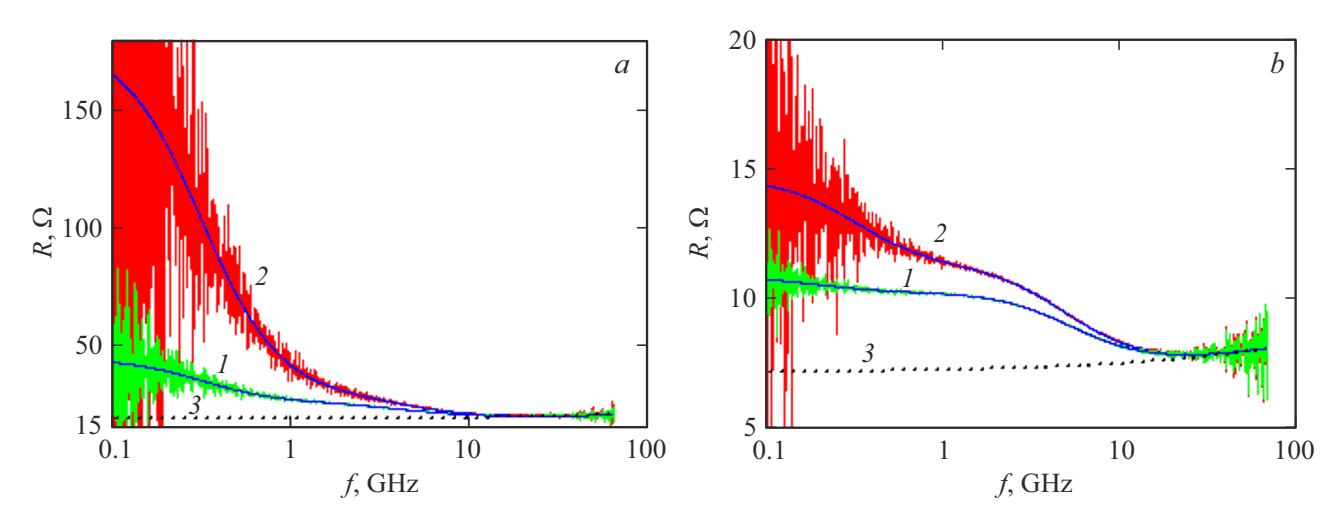


**Figure 2.** Resistance spectra: a — antenna A1, b — antenna A2. U = 0 (I), 4.5 V (2). Solid lines I, 2 — model calculation, dashed line 3 — spectrum r(f).

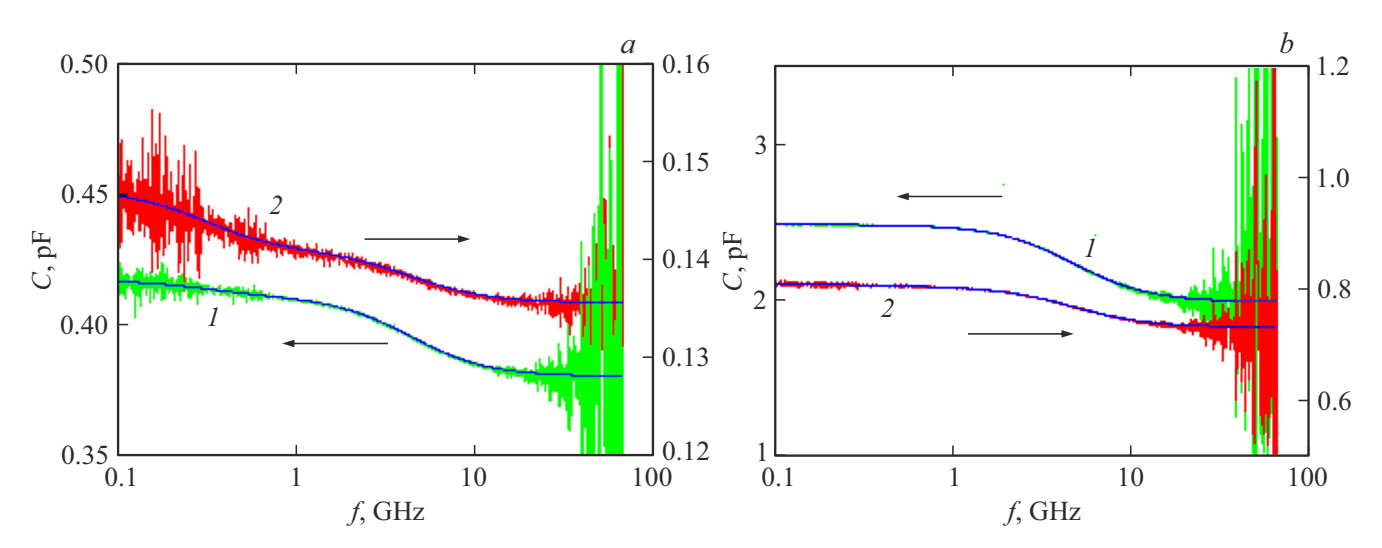


Figure 3. Capacitance spectra: a — antenna A1, b — antenna A2. U = 0 (I), 4.5 V (I). Solid lines I, I0 — model calculation.

runction (4) parameters						
Antenna	U, V	$\tau_h \cdot 10^{11}$ , s	$R_h$ , Ohm	$\tau_l \cdot 10^9$ , s	$R_l$ , Ohm	C <sub>0</sub> , pF
A1	0	3.5	6.8	0.5	19	0.42
	4.5	3.5	9.6	0.5	150	0.15
A2	0	3.0	3.0	0.8	0.7	2.5
	4.5	3.2	4.0	0.5	3.5	0.81

#### Function (4) parameters

resistance R(f) at low frequencies. This feature is caused by the noise of the spectrometer, which was analyzed in detail in the work [21]. Nevertheless, all the features of the spectra R(f,U), C(f,U) can be traced quite clearly in the most informative frequency range at  $f>0.1\,\mathrm{GHz}$ .

In accordance with C-V- and Z-V-diagnostic methods, the dependence of the contact capacitance on the bias voltage C(U) allows determining the concentration of free carriers n. In this case, a n-type semiconductor responds

to a decrease in capacitance with an increase in negative bias. This situation occurs in the considered sample. As can be seen from Figure 3, the specific feature of the SC in the Si sample is that the capacitance C decreases markedly with increasing frequency, which was not observed for the GaAs sample in Ref. [6]. The analysis in Sec. 4 will show that the thickness of the depleted layer d corresponds to the value  $C(f \to \infty, U) = C_{\infty}(U) = \varepsilon_0 \varepsilon' S_a / d(U)$ , where  $\varepsilon_0$ —vacuum electrical constant,  $\varepsilon' = 11.7$  is the dielectric

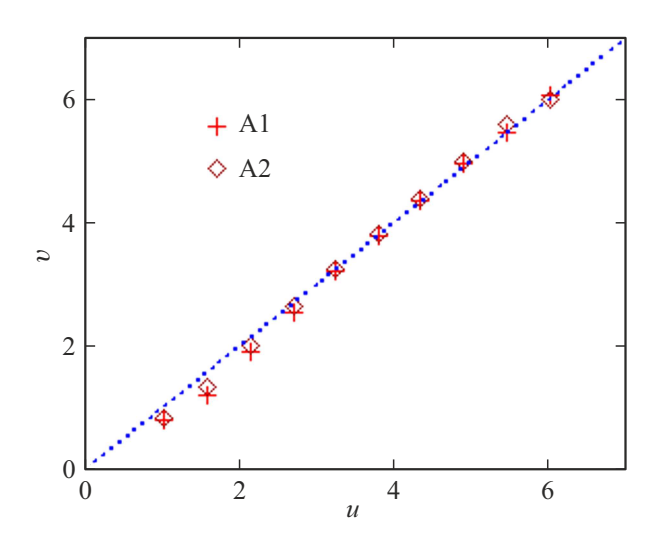


**Figure 4.** Dependence d(U) in normalized variables. Dashed curve — function v=u.

constant of silicon. Figure 4 shows the dependence d(U) obtained from capacitance measurements in normalized variables  $u=U/U_c$ ,  $v=(d/d_0)^2$ . The values of the normalization parameters are determined from the condition of the smallest standard deviation of the experimental data relative to the function v=u. We obtained  $d_0=d(U=0)=98\,\mathrm{nm},\ U_c=0.9\,\mathrm{V}$  in according to the data in Figure 4. In the model of total depletion [23]  $d_0=\sqrt{2\varepsilon'\varepsilon_0U_c/en}$ , where e is the electron charge. As a result, we find the concentration  $n=1.2\cdot 10^{17}\,\mathrm{cm}^{-3}$ , which is in satisfactory agreement with the above result of Hall measurements. At the same time, the mobility is  $\mu=\sigma/(en)\approx 4.7\cdot 10^2\,\mathrm{cm}^2/(\mathrm{V}\cdot\mathrm{s})$ .

The spectra of Z(f, U = 0) were measured at temperatures of T=24, 100 °C for GaAs sample studied in Ref. [6] in addition to the performed studies of the Si sample at room temperature of T = 24 °C. The purpose of these measurements was to identify the dependence  $\tau_{l,h}(T)$ characteristic for deep states (traps), which, as assumed in Ref. [6], determined the observed features of the spectra R(f). Assuming  $\tau(T) = \tau_0 \exp(\Delta/(\kappa T))$ , where  $\Delta$  is the energy of the deep impurity level relative to the bottom of the conduction band,  $\kappa$  is the Boltzmann constant, we obtain  $\tau(T = 297 \text{ K})/\tau(T = 373 \text{ K}) = \exp(6.9 \cdot 10^{-4} \cdot \Delta/\kappa)$ . Thus, when the sample is heated by 76 °C, the time  $\tau$  decreases by more than 2 times at  $\Delta > 86$  meV which is a very likely value at least for traps of l-type. Results of measurement of spectra R(f, U = 0) at T = 24,  $100 \,^{\circ}$ C are shown in Figure 5. We have  $\tau_l(24\,^{\circ}\text{C}) = \tau_l(100\,^{\circ}\text{C}) = 6\cdot 10^{-9}\,\text{s}$ ,  $\tau_h(24\,^{\circ}\text{C}) = 4.2\cdot 10^{-11} \text{ s}, \ \tau_h(100\,^{\circ}\text{C}) = 4.7\cdot 10^{-11} \text{ s}.$  Thus, the expected decrease of  $\tau$  with an increase of T was not detected in the measurements performed. Moreover, we obtained  $\tau_h(100\,^{\circ}\text{C}) > \tau_h(24\,^{\circ}\text{C})$ .

Let's pay attention to one more significant circumstance that contradicts the trap hypothesis. The character of the spectra R(f) turned out to be similar, and the time scales

 $\tau_{l,h}$  were quite close for GaAs and Si samples — an unlikely fact for traps in two significantly different semiconductors. An obvious candidate for traps is an incompletely ionized dopant for a high-frequency effect with a recharge time of  $\tau_h$ . The recharge of a partially ionized dopant is predicted in Ref. [17] and was observed, for example, in Ref. [19]. In our case, the dopants, which differ greatly in the parameter  $\Delta = 5 \text{ meV (S in GaAs)}, 45 \text{ meV (P in Si)}, \text{ should probably}$ also differ in the recharge time  $\tau_h$ , which is not observed in the experiment. In addition, a rather strong change in capacitance was found in the Si sample in the area of the intended effect of h traps (frequency range of  $f > 5 \,\mathrm{GHz}$ in Figure 3). According to the trap theory [15,17,18], the capacitance spectrum  $C(f) = C_{\infty} + \Delta C/(1 + (\omega \tau)^2)$ , where  $\Delta C/C_{\infty} = (C_0 - C_{\infty})/C_{\infty} = \alpha n_t/n$ , parameter  $\alpha < 1$ ,  $n_t$  is the concentration of non-ionized impurity As a result, measurements at U = 0 yield  $n_t/n > 0.1-0.2$ , which is not a realistic estimate for Si at room temperature. Indeed, the condition of electrical neutrality implies the ratio for the concentration of electrons n in the conduction band [23]:

$$n = \frac{n_1}{2} \left( \sqrt{1 + \frac{4N_d}{n_1}} - 1 \right),\tag{5}$$

 $N_d$ is the concentration  $n_1 = (1/2)N_c \cdot \exp(-\Delta/\kappa T)$ ,  $N_c$  is the density of states. Taking for Si  $N_c = 3.2 \cdot 10^{19} \,\mathrm{cm}^{-3}$ ,  $N_d = 10^{17} \,\mathrm{cm}^{-3}$ ,  $\Delta = 45 \,\mathrm{meV}$ ,  $T = 295 \,\mathrm{K}$ , we obtain  $n = 0.97 \cdot 10^{16} \,\mathrm{cm}^{-3}$ . the concentration of non-ionized donors  $n_t/N_d = (1 - n/N_d)$  on  $\sim 3\%$  is significantly less than the concentration obtained from the experiment. However, a similar estimate for GaAs at  $N_c = 4 \cdot 10^{17} \,\mathrm{cm}^{-3}$ ,  $\Delta = 5 \text{ meV}$  gives  $n_t/N_d \sim 30 \%$ . However, such large effects were not observed in the GaAs sample. No change in capacitance was obtained in the measurements presented in Ref. [6], similar to Figure 3. The concentration of  $n_t/N_d$ , which did not exceed 5 %, was estimated from the resistance spectra of R(f), similar to those shown in Figure 2.

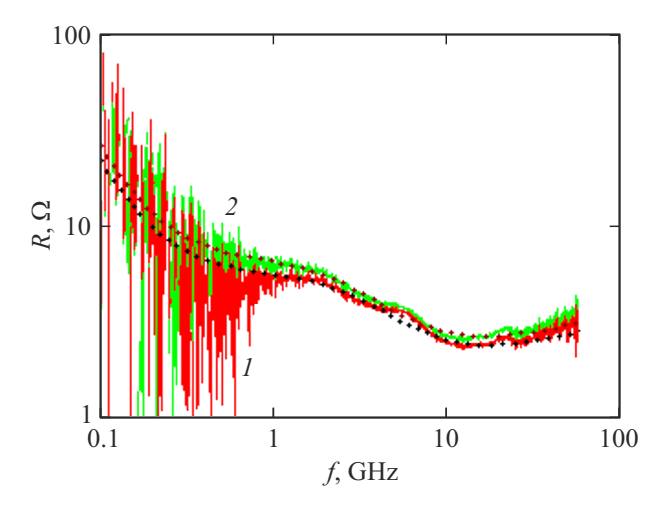


**Figure 5.** The resistance spectrum for the GaAs sample at T = 24 °C (1), 100 °C (2). Dashed curves — calculation result.

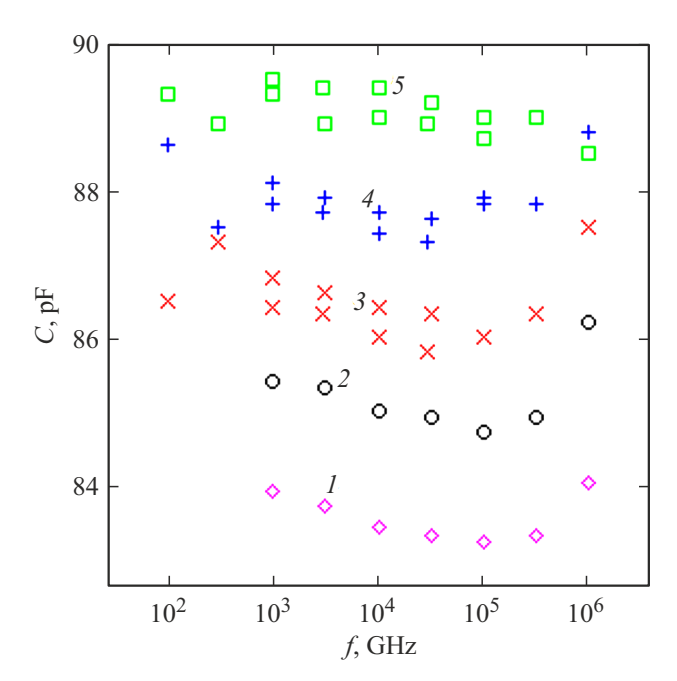


**Figure 6.** Low-frequency capacitance spectra for a GaAs sample at different temperatures T, K: I - 77, 2 - 120, 3 - 150, *4* — 180 and *5* — 210.

#### 3.2. LF measurements

The purpose of the LF studies of the GaAs sample was also to detect traps. The effects of traps in p-n-junctions and SC have often been observed in the  $Y(f) = Z^{-1}(f)$ admittance spectra and have been extensively studied since the 1960s [13–19]. The corresponding research method, called admittance spectroscopy, is implemented with a temperature sweep in the frequency range of  $f < 1 \,\mathrm{MHz}$ with a contact diameter of a > 300 microns. It uses the fact that the recharge time of deep levels increases with decreasing temperature as  $\tau = \tau_0 \exp(\Delta/\kappa T)$ . At the same time, the observed features of the Z(f) spectra are similar to our measurements in Figures 2 and 3. A capacity drop  $C_0 \rightarrow C_\infty$  at  $\tau \sim 10^{-5} - 10^{-6}$  s can be observed at frequencies  $f \sim 1.6 \cdot (10^4 - 10^5) \,\mathrm{Hz} \ (\omega \tau \approx 1)$  falling within the operating range of low-frequency measurements when the sample is cooled to liquid nitrogen temperature. It is estimated that for low-frequency traps  $\Delta C/C_{\infty} \sim 5\%$ ,  $\tau_l(295\,\mathrm{K}) \approx 10^{-9}\,\mathrm{s}$  [6]. Taking  $\tau(77\,\mathrm{K}) = 10^{-5} - 10^{-6}\,\mathrm{s}$ , we have  $\tau (T = 77 \text{ K}) / \tau (T = 295 \text{ K}) \approx \exp(9.6 \cdot 10^{-3} \cdot \Delta / \kappa)$ . As a result, we obtain an estimate of  $\Delta \sim 62.5-84\,\text{meV}$ , corresponding to the state energy of a not very large, but quite acceptable depth for l traps. Deeper states in low frequency measurements can be detected at T > 77 K. Thus, the detection of *l*-traps with a recharge time at room temperature  $\tau_l \sim 10^{-9}$  seemed quite likely when the sample was cooled to nitrogen temperature, which was not confirmed in the LF measurements performed.

The capacitance and resistance spectra obtained at various temperatures are satisfactorily described by the scheme in Figure 1, a with a single time scale  $\tau = R_c C_d$  (1s model). According to this model,  $Z(f) = R_c/(1 + i\omega\tau)$ , since in the low frequency range  $Re(Z) \gg r$ . result, we have  $C(f) = \operatorname{Im}(Y(f)/\omega) = C_d = \operatorname{const}$ , which is confirmed by experimental data in Figure 6, i.e., the capacitance spectra do not contain the expected feature. We obtain  $R(f) = \operatorname{Re}(Y(f)^{-1}) = R_c/(1 + \omega^2 \tau^2)$  for the resistance, which also corresponds to the experimental data in Figure 7, both near room temperature and at higher temperatures. The curves 1-4 in Figure 7 correspond to the resistance  $R_c = 5.2$ , 1.2, 0.38, 0.11 MOhm. The spectrum of R(f) could not be measured using the equipment used at  $T < 270 \, \text{K}$ .

The dependence C(U) of the GaAs sample obtained at room temperature was used to determine the concentration of  $n_f$  using the C-V method, similar to Figure 4. We received  $n_f = 4.8 \cdot 10^{16} \, \text{cm}^{-3}$ , which is noticeably higher than the result of the microwave Z-V diagnostics  $n_f = 4.1 \cdot 10^{16} \,\mathrm{cm}^{-3}$  in the article [6] with the same value  $U_c = 0.88$  V. Figure 3 shows that the capacity  $C_0$ , measured in the range f < 1 GHz, exceeds  $C_{\infty}$  for the Si sample. As a result, we have  $d(f \to 0) < d(f \to \infty)$ , which is why for concentration  $n(f \to 0) > n(f \to \infty)$ . Indeed, the usage of the dependence  $C_0(U)$  in the spectra C(f) in Figure 3 leads to an overestimation of  $n = 1.4 \cdot 10^{17} \, \mathrm{cm}^{-3}$  with the same parameter  $U_c = 0.9 \,\mathrm{V}$  (compare with the concentration of  $n = 1.2 \cdot 10^{17} \,\mathrm{cm}^{-3}$  obtained in section 2.1). At the same time, the transition  $C_0 \rightarrow C_{\infty}$  in the range  $f > 0.01 \, \text{GHz}$ was not observed for the GaAs sample in Ref. [6], as well as

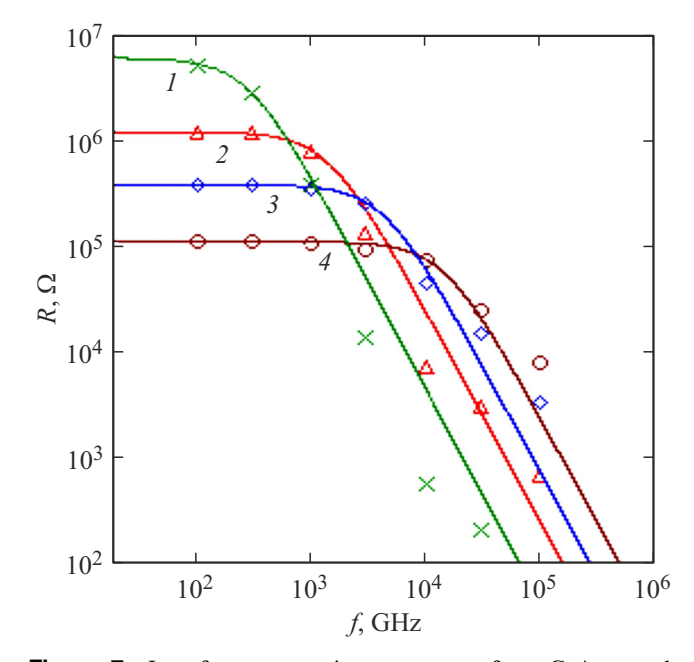


Figure 7. Low-frequency resistance spectra for a GaAs sample at different temperatures T, K: 1-275, 2-297, 3-320 and 4 — 345. Icons — experimental data, solid lines — calculation according to the scheme in Figure 1, a.

in the low-frequency measurements at f < 1 MHz, that is, the change in capacitance falls within the frequency range f = 1-100 MHz, where the spectrum C(f) has not been measured. The mechanism of changing the capacitance for Si and GaAs samples is different and in the latter case may be due to the recharge of traps. It is likely that the transition  $C_0 \to C_\infty$  at  $\omega \tau \cong 1$  is realized in the specified frequency range, i.e., the recharge time of the non-ionized donor impurity S in GaAs  $\tau \sim 10^{-8}$  s at room temperature. As shown in Section 3.1, the concentration of the non-ionized donor impurity is quite high for GaAs, which is why this impurity must act as traps. Then the transition  $C_0 \to C_\infty$  at frequencies  $10^2-10^6$  Hz can be observed at T < 77 K. Measurements at such temperatures were not carried out in this study.

#### 4. MW model — interpretation

The hypothesis expressed in Refs. [5,6] about the connection of excessive resistance with the recharging of traps has not been confirmed based on the results of the above studies. Further, another explanation is proposed, according to which the observed features of the MW spectrum Z(f) may be associated with the transport of residual charge carriers in the depleted region, the concentration of which n(x, U) is determined by the equation

$$n(x, U) = n_0 \exp\left\{\frac{e}{\kappa T} \left[\varphi(x) - (U_c + U)\right]\right\}, \quad (6)$$

where the potential distribution  $\varphi(x)$  is found from the solution of the Poisson equation with the corresponding boundary conditions [23]:

$$\frac{d^2\varphi}{dx^2} = \frac{en_0}{\varepsilon_0\varepsilon'} \left\{ \exp \frac{e(\varphi - (U_c + U))}{\kappa T} - 1 \right\}. \tag{7}$$

The undisturbed concentration  $n(x \to \infty)$  in (6), (7) is now denoted as  $n_0$ . The thickness of the depleted region  $d(U) = d_0(1 + U/U_c)^{1/2}$  is in the approximation of total depletion, suggesting an abrupt change in concentration n at the boundary x = d:

$$n(x) = \begin{cases} 0, & x \le d \\ n_0, & x > d \end{cases},$$

as a result, on the right side of the equation (7) the exponential term is excluded, and the thickness of  $d_0$  is determined by the expression given in section 3.1, which is used to find the concentration of  $n = n_0$ . The impedance of the depleted SC layer at  $d(U) \ll a$  (one-dimensional geometry) is given by the following expression:

$$Z_{S}(f) = \int_{0}^{d} \frac{dx}{\sigma_{c}(x, f)} \cdot \frac{1}{S_{a}},\tag{8}$$

where  $\sigma_c$  is the complex conductivity, which in semiconductors in the radio frequency range is usually determined by a

relation that takes into account conduction and displacement currents:

$$\sigma_c(x, f) = e\mu n(x) + i2\pi f \varepsilon_0 \varepsilon'. \tag{9}$$

The expression (9) is not accurate in SC, since in addition to the drift current, the diffusion current plays an essential role in the material response, and it is also necessary to take into account the variable component of the drift current associated with the built-in constant electric field  $E_{dc} = -d\varphi/dx$  in (7). In the drift-diffusion approximation, the alternating conduction current  $\tilde{J}$  and concentration  $\tilde{n}$  for one-dimensional transport are related to the alternating electric field  $\tilde{E}$  by the relations [24,25]:

$$\tilde{j}(x) = e\mu n(x)\tilde{E} + \mu\kappa T \frac{d\tilde{n}}{dx} + e\mu E_{dc}\tilde{n},$$
 (10a)

$$\frac{d\tilde{E}}{dx} = -\frac{e}{\varepsilon'\varepsilon_0}\tilde{n}.$$
 (10b)

In equation (10a), as well as in (9), it is assumed that  $\omega \ll \nu$ , where  $\nu$  is the collision frequency. the formula (9) for qualitative analysis of the impedance spectrum (8), which takes into account only the first term on the right side of equation (10a). A similar approach was applied in Ref. [25] to explain the physical nature of the effects of carrier transport in SC. In the same work, a study was performed based on the complete system of equations (10), which confirmed the qualitative analysis. Applying the mean value theorem to (8), we can write  $Z_S(f) = (1/(\sigma_d + i\omega\varepsilon_0\varepsilon))(d/S_a)$ . The above formula also follows from 1s the depleted area scheme in Figure 1, a, in which  $R_c = d/(\sigma_d S_a)$ ,  $C_d = \varepsilon_0 \varepsilon' S_a/d$ without series resistance r (3), which is formed by the area x > d and is not included in (8). According to the LF measurements performed for the GaAs sample,  $C_d = 94 \,\mathrm{pF}$ ,  $R_c = 1.2 \,\mathrm{MOhm}$  at U = 0,  $T = 297 \,\mathrm{K}$ . Taking  $\varepsilon' = 12.9$ , fact, the circuit 1s replaces the effective conductivity  $\sigma_{ef}(x, f) = \text{Re}(\sigma_c(x, f))$  in (8) with a certain constant value  $\sigma_d$ , uniformly distributed throughout the depleted layer and independent of frequency f.

Using the formula (9), we consider the Joule losses dQ(x) in the elementary section dx of the depleted layer, which is characterized by parallel connected resistance  $dR = dx/(\sigma_{ef}(x)S_a)$  and reactance  $dX = dx/(i\omega\varepsilon_0\varepsilon'S_a)$ . If an alternating current with an amplitude of  $I_{\sim}$  flows through the layer, then  $dQ(x) = (1/2)|I_{\sim}|^2J(x)dx/S_a$ , where

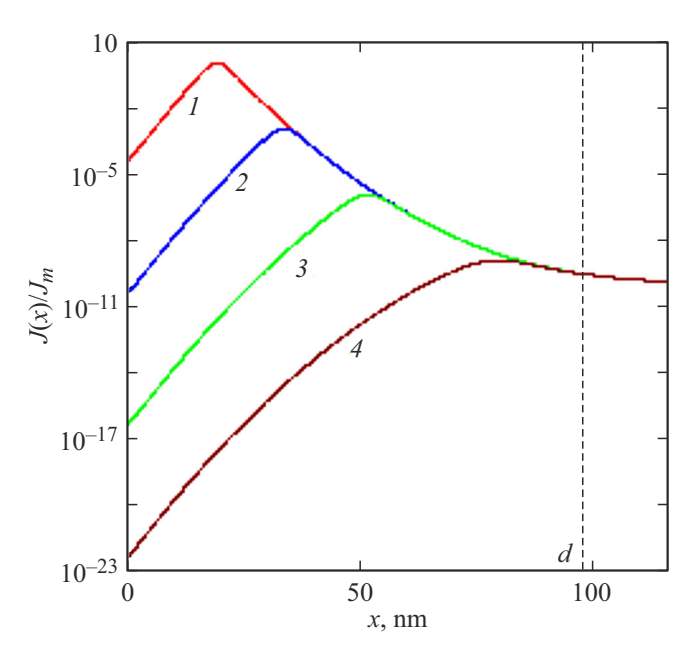
$$J(x) = \frac{\sigma_{ef}(x)}{|\sigma_{ef}(x) + i\omega\varepsilon_0\varepsilon'|^2}.$$
 (11)

Figure 8 shows the distribution of  $J(x)/J_m$  at various frequencies of the range  $10^2-10^{11}$  Hz, where the normalizing factor  $J_m$  is the maximum value of the function J(x) at  $f=10^2$  Hz, and in the formula (9)  $\mu=5\cdot 10^2$  cm<sup>2</sup>/(V·s). The concentration of n(x) in (9) is calculated using the equations (6), (7) at  $n_0=1.2\cdot 10^{17}$  cm<sup>-3</sup>, U=0,  $U_c=0.9$  V,  $\varepsilon'=11.7$ . It can be seen that in the low

frequency range  $f=10^2-10^5$  Hz, losses are formed in the region  $x < l_{lf} = 30-50\,\mathrm{nm}$  adjacent to the metal boundary x=0. This area defines a very low average conductivity  $\sigma_d$  and a high resistance  $R_c$ , as here  $n(x) \ll n_0$ . According to measurements of the GaAs sample in Ref. [6]  $\sigma=8.1~(\mathrm{Ohm\cdot cm})^{-1}$  at  $n_0=4.1\cdot 10^{16}~\mathrm{cm}^{-3}$ ,  $\mu=1.2\cdot 10^3~\mathrm{cm}^2/(\mathrm{V\cdot s})$ . As expected, we obtained  $\sigma_d\ll\sigma$ . Despite the assumption made for calculating the integral (8), the circuit 1s satisfactorily describes the experimental LF spectra in Figures 6 and 7.

As can be seen from Figure 8, the character of the function J(x) changes dramatically in the MW band. It is possible to distinguish layer l < d near the "far" boundary of the depleted layer x = d, in which the main losses are concentrated. The region x < d - l does not contribute to losses, since the resistance of this region  $R \sim R_c$  at MW frequencies is shunted by the capacity  $C_0$  in the formula (4). Thus, the residual carriers in the depleted layer with a concentration of  $n(x) < n_0$  contribute to losses, i.e., they can form excessive resistance in the MW range. An approximate calculation of the integral (8), similar to the calculation of the low-frequency impedance, does not, however, give the spectrum Z(f) corresponding to the experimental data in Figures 2 and 3. In accordance with 2s model (4), the layer l is divided into two sublayers  $l_l + l_h = l$ ,  $R_{l,h} = l_{l,h}/(\sigma_{l,h}S_a), \ \tau_{l,h} = R_{l,h}C_{l,h}, \ C_{l,h} = \varepsilon_0 \varepsilon' S_a/l_{1,h}.$  Using the data in the table, for sample Si and antenna A1 at U = 0 we find:  $\sigma_l = 2.1 \cdot 10^{-3} \, (\text{Ohm} \cdot \text{cm})^{-1}$ ,  $l_l = 1.2 \, \text{nm}$ ,  $\sigma_h = 3 \cdot 10^{-2} \, (\text{Ohm} \cdot \text{cm})^{-1}$ ,  $l_h = 6.4 \, \text{nm}$ . The structure of the effective conductivity of the sample  $\sigma_{ef}(x)$ , corresponding to the 2s scheme, is qualitatively shown in Figure 8, which also shows the conductivity  $\sigma_d$ , which determines the resistance  $R_c$  of this scheme. It can be seen that  $d = d_{HF} = (\varepsilon_0 \varepsilon' S_a / C_\infty) = 85.6 \,\mathrm{nm}$  is the thickness of the depleted layer, whereas for the capacity  $C_0$  in the formula (4) we obtain  $d_{LF} = (\varepsilon_0 \varepsilon' S_a / C_0) = 78 \,\text{nm}$ , with  $d_{HF} = d_{LF} + l_l + l_h$ . The given  $d_{HF}$  value slightly differs from the thickness  $d_0$  obtained in Section 3.1 from the data in Figure 4, since this figure corresponds to the average value of the parameter  $d_0$  for all voltages Ufor both antennas. It should be noted that due to the ratio  $J(x)^{\mbox{MW}} \ll J(x)^{\mbox{LF}}$  in Figure 8, we have  $R_{l,h} \ll R_c$ ,  $\tau_{l,h} \ll \tau$  in the MW and LF models. Figure 1, b shows the MW Schottky diode circuit corresponding to the 2s model (4) at  $R_c \gg (\omega C_0)^{-1}$ . This circuit is also valid for the LF range, since here  $R_{l,h} \ll (\omega C_{l,h})^{-1}$ ,  $R_c \gg R_{l,h}$ , i.e., we come to the circuit in Figure 1, a with substitutions  $C_d \rightarrow C_0$ ,  $r \rightarrow R_l + R_h + r$ . The last substitution does not play a fundamental role, since in low-frequency measurements, the resistance  $R(f) = R_c/(1 + \omega^2 \tau^2) \gg r$ ,  $R_{l,h}$ .

Let's pay attention to the abnormal dependence of the excess resistance parameters  $R_{l,h}$  in the formula (4) on the diameter of the antenna a. As can be seen from the table, the expected dependence  $R_{l,h}(U) \sim a^{-2}$  is not realized, while other parameters of this formula correspond to expectations —  $C_0(U) \sim a^2$ ,  $r \sim a^{-1}$ . We also have  $C_{\infty}(U) \sim a^2$  for the capacity at  $f \to \infty$ . It is possible that



**Figure 8.** Distribution of Joule losses in SC. Frequency  $f = 10^2 (1)$ ,  $10^5 (2)$ ,  $10^8 (3)$ ,  $10^{11} (4)$  Hz.

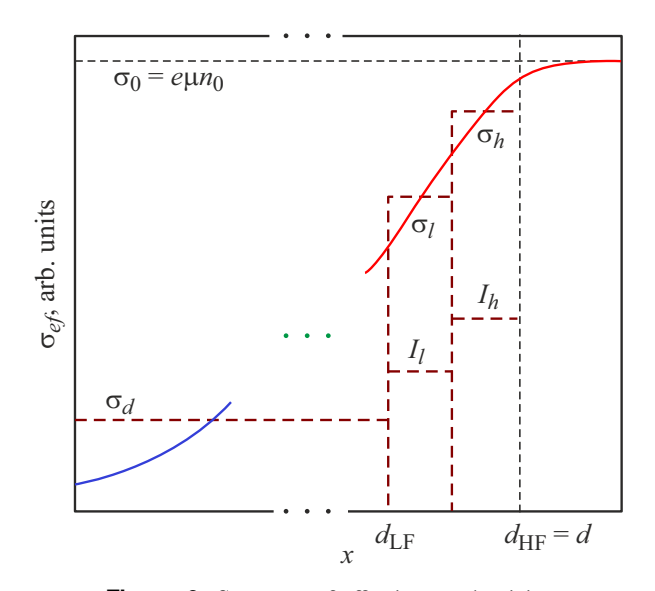


**Figure 9.** Structure of effective conductivity.

the three-dimensional structure of the alternating current in the undisturbed region of the semiconductor x > d is affected. For the GaAs sample in Ref. [6], the dependencies  $R_{l,h}(U) \sim a^{-2}$  were performed with good accuracy.

In the proposed 2s circuit, the unknown effective conductivity of the depleted layer  $\sigma_{ef}(x) = \text{Re}\left(\sigma_c(x)\right)$  in (8) is substituted by a step function in Figure 9 with average values  $\sigma_{l,h}$  in layers  $l_{l,h}$ . As it turned out, this approximation makes it possible to adequately describe experimental MW spectra without involving the trap hypothesis. Our more general assumption is that in the depleted SC layer, due to the peculiarities of carrier transport, a continuous distribution

of conductivity  $\sigma_c(x, f)$  is realized, in which the impedance  $Z(f) = Z_S(f) + r(f)$  is calculated using the formula (8) gives the experimental spectra in Figures 2 and 3.

There are theoretical studies of carrier transport in the SC in an alternating electric field in the literature. For instance, the linear and nonlinear high-frequency response of a Schottky diode is studied in Ref. [26] based on the solution of the kinetic equation and the Poisson equation. The ballistic transport of charge carriers in SC is considered when the mean free path is  $l_n \gg d$ . The authors proposed an interpolation formula for the admittance of a depleted region of the form:

$$Y_S(\omega) = j\omega C_d + \frac{1}{R_c(1 + (\omega/\omega_p)^2)},$$
 (12)

where  $\omega_p=2\pi f_p$  is the plasma frequency in the quasineutral region. The spectrum (12) is not described by the 1s circuit in Figure 1, a in the frequency range  $\omega > \omega_p$ , significantly exceeding the operating frequencies of formula (4), since for our sample  $f_p \sim 1-10\,\mathrm{THz}$ . It should be noted that the authors of Ref. [26] considered only the highfrequency asymptotics of admittance, whereas the region of intermediate frequencies  $\tau^{-1} < f < f_p$  in formula (12) is described intuitively as an interpolation stitching of the lowfrequency and high-frequency parts of the spectrum  $Y_S(\omega)$ . The SC impedance was calculated in Ref. [24] based on the drift-diffusion equations (10), which characterize carrier transport in the depleted layer at  $d \gg l_n$ . The authors concluded that the circuit in Figure 1, a does not describe the MW spectrum Z(f) already in the frequency range of our measurements  $f > 0.1 \,\text{GHz}$ . However, the calculation of the static electric field in the 0th order of perturbation theory was performed in the approximation of total depletion, which leads to a large error near the boundary of the quasineutral region. Moreover, if the thin region  $l \sim l_n$  adjacent to the far boundary of the depleted layer (see Figure 9) plays the main role in the formation of the obtained MW effects in the SC, then transport in this area is not described by driftdiffusion equations. Apparently, there is an intermediate mechanism of transport with a small number of acts of Thus, the models developed in the carrier scattering. literature cannot be considered sufficiently adequate.

The performed analysis suggests that the effects obtained in this work and in Refs. [5,6] may be related to the peculiarities of charge carrier transport in the depleted SC layer. Theory of this transport requires further development.

#### 5. Conclusion

Summing up the conducted studies, we list the main provisions according to which the relation of excessive resistance with the recharging of traps, proposed in Refs. [5,6] as a hypothesis, now does not seem convincing enough

1) two significantly different samples based on GaAs and Si have similar resistance spectra R(f);

- 2) there should not be any excessively strong high-frequency effect in the Si sample at a low relative concentration of non-ionized donors;
- 3) the expected dependence of time scales  $\tau$  on temperature T in the spectra of Z(f,T) was not observed when the sample was heated;
- 4) there was no transition  $C_0 \to C_\infty$  characteristic of traps in the low-frequency spectra C(f) when the GaAs sample was cooled to the temperature of liquid nitrogen.

A possible cause of the observed MW effects is deceleration and dissipation during transport of residual charge carriers in the SC depleted layer. The proposed 2s circuit is a consequence of the approximate calculation of the integral (8) with the complex conductivity  $\sigma_c(x, f)$  determined by this transport. It is assumed that the distribution of conductivity realized in SC gives the obtained experimental spectra of Z(f, U).

Optimal conditions for observing excessive resistance are realized in the frequency range  $f>0.5\,\mathrm{GHz}$  with a contact diameter  $a<100\,\mathrm{microns}$  in the planar geometry of the antenna system. The lower frequencies are not informative enough in relation to the studied effects. In addition, the noise of the spectrometer makes it difficult to measure the spectrum of R(f) in the range of  $f<0.1\,\mathrm{GHz}$ , as can be seen from Figure 2. A comparison of Figure 2, a and b shows that with increasing diameter a, the excess of resistances  $R_{l,h}$  over r in (4) decreases. Spectrum  $r(f)>R_{l,h}$  masks excessive resistance at  $a>100-200\,\mathrm{microns}$ . All the listed conditions are fulfilled in the studies conducted here, like in previous papers [5,6].

In this paper, using a Si sample, we demonstrated the possibility of determining a complete set of electrophysical parameters of a semiconductor by local MW spectroscopy. The same conclusion was made in our previous papers [4,6] based on the results of studies of a homogeneous plate and planar structure on GaAs. The lateral resolution of 10-60 microns we implemented can be improved to 3-5 microns and is limited by the characteristics of modern PS. Currently, significantly better resolution of MW diagnostics (up to 30–50 nm) is achieved for SMM [9–12]. In recent studies [27–30], the authors came to an optimistic conclusion regarding the determination of the concentration n in a semiconductor using nanoresolution SMM. This conclusion contradicts an earlier study in Ref. [31], where absolute measurements of n were performed with an accuracy of only an order of magnitude due to the influence of the oxide film on the semiconductor surface. It should also be noted that a semiconductor differs significantly from other materials at the nanoscale (metals, dielectrics, etc.). Due to the cold emission of electrons and the presence of surface states, a 20-200 nm layer with a disturbed concentration of n (depleted or enriched) is formed at the surface of the semiconductor [23]. An SMM probe placed at a distance of  $\sim 1\,\mathrm{nm}$  to the surface distorts the characteristics of this layer. Adequate consideration of these circumstances is necessary for semiconductor nanodiagnostics, but has not been carried out in the

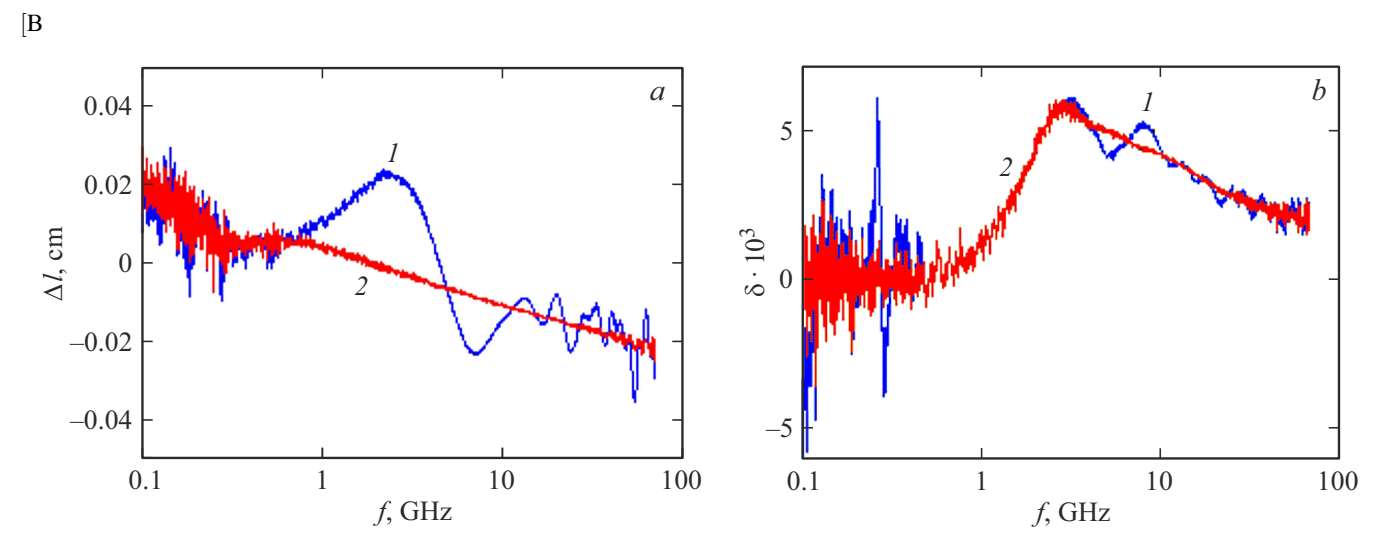


**Figure A.1** Spectra of the electrical length amendment (a) and loss parameter (b) of the probe: I — initial spectra, 2 — adjusted spectra.

publications cited above. SMM of medium resolution (no better than 85 microns) was used for semiconductor diagnostics in Refs. [32–35]. For such a device, the effect of the disturbed nanometer layer is significantly reduced, as a result of which the demonstrated possibility of determining the electrical conductivity  $\sigma$  of a homogeneous material or the sheet resistance of the film structure seems justified. The method of local MW spectroscopy developed by us forms in a semiconductor a depleted surface layer with controlled characteristics, which is described by the classical SC theory. This made it possible, along with  $\sigma$ , to determine the concentration of carriers n, and therefore their mobility  $\mu$ . In contrast to the selective SMM operating frequency, reliable measurements with the spectrometer were performed in the wide frequency band 0.1-67 GHz. As a result, the information content of the diagnosis has increased, which made it possible not only to determine the electrophysical characteristics, but also to detect and investigate excessive resistance.

### **Appendix**

#### Correction of experimental spectra

The source of information about the parameters of the test sample are the Z(f,U) spectra, which are reconstructed from the spectrum of the complex reflection coefficient  $\Gamma(f)=A(f)\cdot\exp(i\varphi(f))$  measured at the MW probe input. An important intermediate task is to convert the function  $\Gamma(f)$  into the function  $G(f)=(Z(f,U)-Z_{CM})/(Z(f,U)+Z_{CM})$ , which is the reflection coefficient in the plane of the plate with which the probe is brought into contact. If the probe is perfectly matched with the waveguide path of the PS, then for the SM station, its wave impedance  $Z_{CM}=50\,\mathrm{Ohm}$ . The spectrum Z(f,U) is reconstructed by the AK method

proposed in Ref. [6], according to which the probe is modeled by a segment of a waveguide line of length  $l_{CM}$ with a wavenumber  $k_{CM}(f) = (\omega/c)n_{CM}(f)(1-i\delta(f)),$ where  $n_{CM}$  is the effective refractive index,  $\delta$  is the line loss parameter. The PS calibration now boils down to determining the functions  $\delta(f)$  and the electrical length  $l_e(f) = n_{CM}(f)l_{CM}$ . For this purpose, the coefficient  $\Gamma_a(f)$ is measured in the absence of probe-sample contact (Air mode), i. e., reference loads are not used. The AK method is described and studied in detail in Ref. [21]. The calibration spectra  $\Delta l_e(f) = l_e(f) - \langle l_e \rangle$ ,  $\delta(f)$  obtained in the studies of Si sample are shown in Figure A.1 ( $\langle l_e \rangle = 3.045 \, \mathrm{cm}$  is the frequency averaged electrical length of the probe). Both spectra (curves 1) exhibit parasitic high-frequency oscillations caused by oscillations in the initial calibration spectra  $A_a(f)$ ,  $\varphi_a(f)$  (curves 1 in Figure A.2). oscillations are caused by imperfect matching of the probe, i.e.  $Z_{CM} \neq 50 \text{ Ohm } [21]$ . Figure A.2, b shows the phase increment  $\Delta \varphi_a(f) = \varphi_a(f) + 2(\omega/c)\langle l_e \rangle$ , where  $\varphi_a < 0$ , with  $\varphi_a(f = 67\,\mathrm{GHz}) \approx -84$ . In this paper, we draw attention to the possibility of correcting experimental data by smoothing parasitic oscillations, which led to a significant improvement in the spectra of R(f), C(f), shown in Figures 2 and 3 for Si sample.

The noise Smoothing is performed as follows. component of the signal  $\xi_A(f) = A(f) - A_{sm}(f),$  $\xi_{\omega}(f) = \varphi(f) - \varphi_{sm}(f)$  is distinguished in the spectra A(f),  $\varphi(f)$ . Here  $A_{sm}(f)$ ,  $\varphi_{sm}(f)$  is the result of processing the functions A(f),  $\varphi(f)$  with the ksmooth subroutine from the Mathcad package, which removes the noise of the spectrometer without affecting the oscillator component. The functions  $A_{sm}(f)$ ,  $\varphi_{sm}(f)$  are processed by a separate program that removes spurious oscillations. components are added to the resulting functions  $A_s(f)$ , The resulting spectra  $A_n(f) = A_s(f) + \xi_A(f)$ ,  $\varphi_n(f) = \varphi_s(f) + \xi_{\varphi}(f)$  (curves 1c in Figure A.2) are

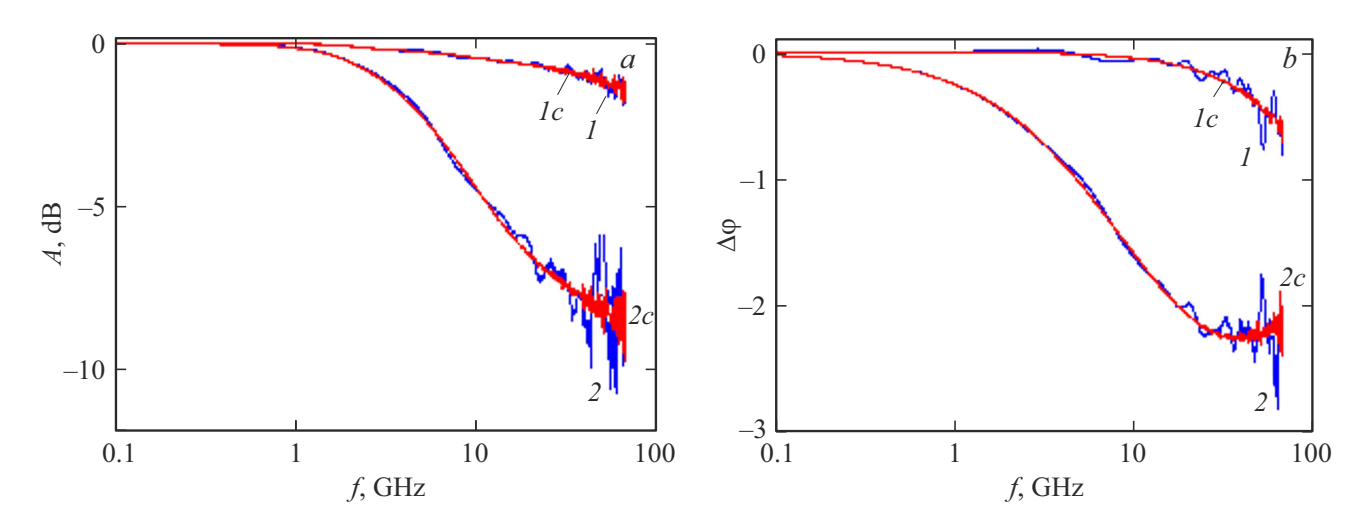


**Figure A.2** Spectra of amplitude (a) and phase increment (b) of the reflection coefficient: I — calibration spectra (Air), 2 — spectra of the Si sample (antenna A1, U=0). Original spectra are shown without index, corrected spectra are shown with index "c".

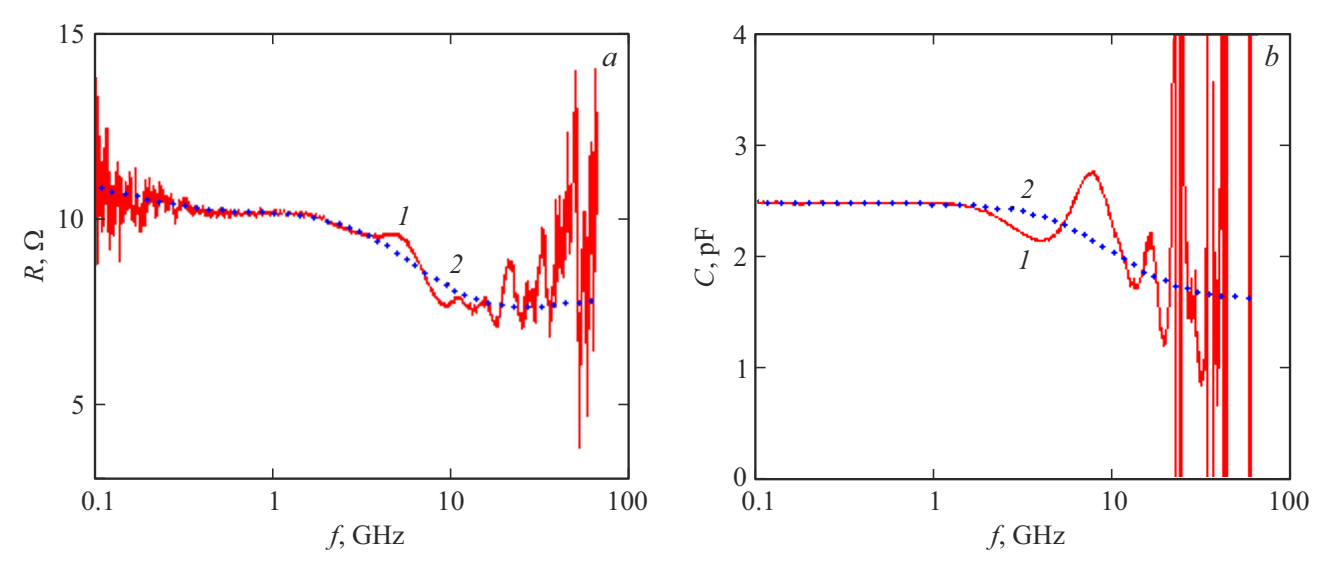


**Figure A.3** Spectra of resistance (a) and capacitance (b). Antenna A2, U=0. Curves I — spectra without correction, 2 — calculation by formula (4).

considered as adjusted experimental data corresponding to a perfectly matched probe  $Z_{CM}=50$  Ohm. Adjusted spectra are determined from these data  $l_n(f)=\Delta l_n(f)+\langle l_e\rangle$ ,  $\delta_n(f)$  (Figure A.1, curves 2). The spectra A(f),  $\varphi(f)$  obtained in probe-sample contact are processed similarly (Figure A.2, curves 2 and 2c). The corrected spectra are used to restore the characteristics of the sample R(f), C(f) (see Figures 2 and 3) using the functions  $l_n(f)$ ,  $\delta_n(f)$  in the AK method.

Examples of the spectra R(f) and C(f) reconstructed by the AK method without correction of experimental data are shown in Figure A.3. A comparison with Figures 2 and 3 shows significant distortions of the high-frequency part of the spectra due to parasitic oscillations in the spectra A(f),  $\varphi(f)$ . Correction of experimental data eliminates these distortions. It is important to note that the main features

of the functions R(f), C(f) are also observed in distorted spectra. These include excessive resistance in the spectrum R(f) with two time scales  $\tau_{l,h}$ , transition  $C_0 \to C_\infty$  in the spectrum C(f).

### **Funding**

This study was supported by the Ministry of Science and Higher Education of the Russian Federation (project FFUF-2024-0042).

#### **Acknowledgments**

The authors are grateful to S.A. Kraev and E.A. Arkhipova, who manufactured the antenna system for the studied samples; V.B. Shmagin and S.A. Korolev, who

performed low-frequency and Van der Pauw measurements. The equipment of the Center of Shared Use of the Institute for Physics of Microstructures of RAS "Physics and Technology of micro- and nanostructures" was used.

#### Conflict of interest

The authors declare no conflict of interest.

#### References

- [1] S.M. Sze, K.K. Ng. *Physics of semiconductor devices. 3rd ed.* (Johen Wiley and Sons, Inc., 2007).
- [2] D.K. Schroder. Semiconductor material and device characterization. 3rd ed. (John Wiley and Sons, Inc., 2006).
- [3] A.N. Reznik, N.K. Vdovicheva. ZHTF, 89 (11), 1813 (2019).
- [4] A.N. Reznik, N.V. Vostokov, N.K. Vdovicheva, V.I. Shashkin. ZHTF, 90 (11), 1944 (2020).
- [5] A.N. Reznik, N.V. Vostokov. ZHTF, 92 (3), 492 (2022).
- [6] A.N. Reznik, N.V. Vostokov. FTP, 57 (3), 169 (2023).
- [7] A. Rumiantsev, R. Doerner. IEEE Microwave Mag., 14 (7), 46 (2013).
- [8] A.Rumiantsev. On Wafer Calibration Techniques Enabling Accurate Characterization of High-Performance Silicon Devices at the mm-Wave Range and Beyond (Denmark, River Publishers, 2019).
- [9] A. Imtiaz, T.M. Wallis, P. Kabos. IEEE Micrwave Mag., 15, 52 (2014).
- [10] S. Berweger, T.M. Wallis, P. Kabos. IEEE Micrwave Mag., 21 (10), 36 (2020).
- [11] Z. Chu, L. Zheng, K. Lai. Ann. Rev. Mater. Res., 50 (1), 105 (2020).
- [12] A. Tseliov. IEEE Micrwave Mag., 21 (10), 72 (2020).
- [13] C.T. Sah, V.G.K. Reddi. IEEE Trans. Electron Dev., **11**, 345 (1964)
- [14] E. Schibli, A.G. Milnes. Solid-State Electron., 11, 323 (1968).
- [15] W.G. Oldham, S.S. Naik. Solid-State Electron., 15, 1085 (1972).
- [16] M. Beguwala, C.R. Crwell. Solid-State Electron., 17, 203 (1974).
- [17] G. Vincent, D. Bois, P. Pinard. J. Appl. Phys., 46, 5173 (1975).
- [18] J.L. Pautrat, B. Katirciogly, N. Magnea, D. Bensahel, J.C. Pfister, L. Revoil. Solid-State Electron., 23, 1159 (1980).
- [19] A.V. Murel, V.B. Shmagin, V.L. Kryukov, S.S. Strelchenko, E.A. Surovegina, V.I. Shashkin. FTP, 51 (11), 1538 (2017). (in Russian).
- [20] M. Hiebel. Fundamentals of Vector Network Analysis (Rohde and Schwarz, 2007).
- [21] A.N. Reznik. Izv. vuzov. Radiofizika, 67 (7), 607 (2024).
- [22] L.E. Dickens. IEEE Trans. Microwave Theory Tech., 15, 101 (1967).
- [23] V.L. Bonch-Bruevich, S.G. Kalashnikov. Physics of Semiconductors VEB. Berlin, 1982.
- [24] D.W. Tsang, S.E. Schwarz. J. Appl. Phys., **50** (5), 3459 (1979).
- [25] M. El-Gabaly. J. Appl. Phys., 55 (2), 571 (1984).
- [26] N.A. Mordovets, A.Ya. Shulman. ZHTF, 56 (11), 2189 (1986).
- [27] O. Amster, F. Stanke, S. Friedman, Y. Yang, St.J. Dixon-Warren, B. Drevniok. Microelectron. Reliab., **76**, 214 (2017).
- [28] S. Berweger, G.A. MacDonald, M. Yang, K.J. Coakley, J.J. Berry, K. Zhu, F.W. DelRio, T.M. Wallis, P. Kabos. Nano Lett., 17, 1796 (2017).

- [29] A. Buchter, J. Hoffman, A. Delvallee, E. Brinciotti, D. Hapiuk, C. Licitra, K. Louarn, A. Arnoult, G. Almuneau, F. Piquemal, M. Zeier, F. Kienberger. Rev. Sci. Instrum., 89, 023704 (2018).
- [30] X. Guo, X. He, Z. Degnan, B.C. Donose, K. Bertling, A. Fedorov, A.D. Rakic, P. Jacobson. Appl. Phys. Lett., 119, 091101 (2021).
- [31] H.P. Huber, I. Humer, H. Hochleitner, M. Fenner, M. Moertelmaier, C. Rankl, A. Imtiaz, T.M. Wallis, H. Tanbakuchi, P. Hinterdorfer, P. Kabos, J. Smoliner, J.J. Kopanski, F. Kienberge. J. Appl. Phys., 111, 014301 (2012).
- [32] A.N. Reznik, E.V. Demidov. J. Appl. Phys., 113, 094501 (2013)
- [33] A.N. Reznik, S.A. Korolyov. J. Appl. Phys., 119, 094504 (2016).
- [34] A.N. Reznik, S.A. Korolyov, M.N. Drozdov. J. Appl. Phys., 121, 164503 (2017).
- [35] S.A. Korolyov, A.N. Reznik. Rev. Sci. Instrum., 89, 023706 (2018).

Translated by A.Akhtyamov